BNL-NUREG-32617
CONF-830805--18

BNL-NUREG--32617

DE83 010456

Nonlinear Finite-Element Analysis of a Reinforced-Concrete Mark III Containment Under Pressure and Gravity Loads*

By

S. Sharma, M. Reich and S. Shteyngart
Department of Nuclear Energy
Brookhaven National Laboratory
Upton, NY 11973, USA

and

T. Y. Chang
Department of Civil Engineering
University of Akron
Akron, OH 44304, USA

MASTER

*This work was performed under the auspices of the U.S. Nuclear Regulatory Commission under contract no. DE-AC02-76CH00016.

List of Figures

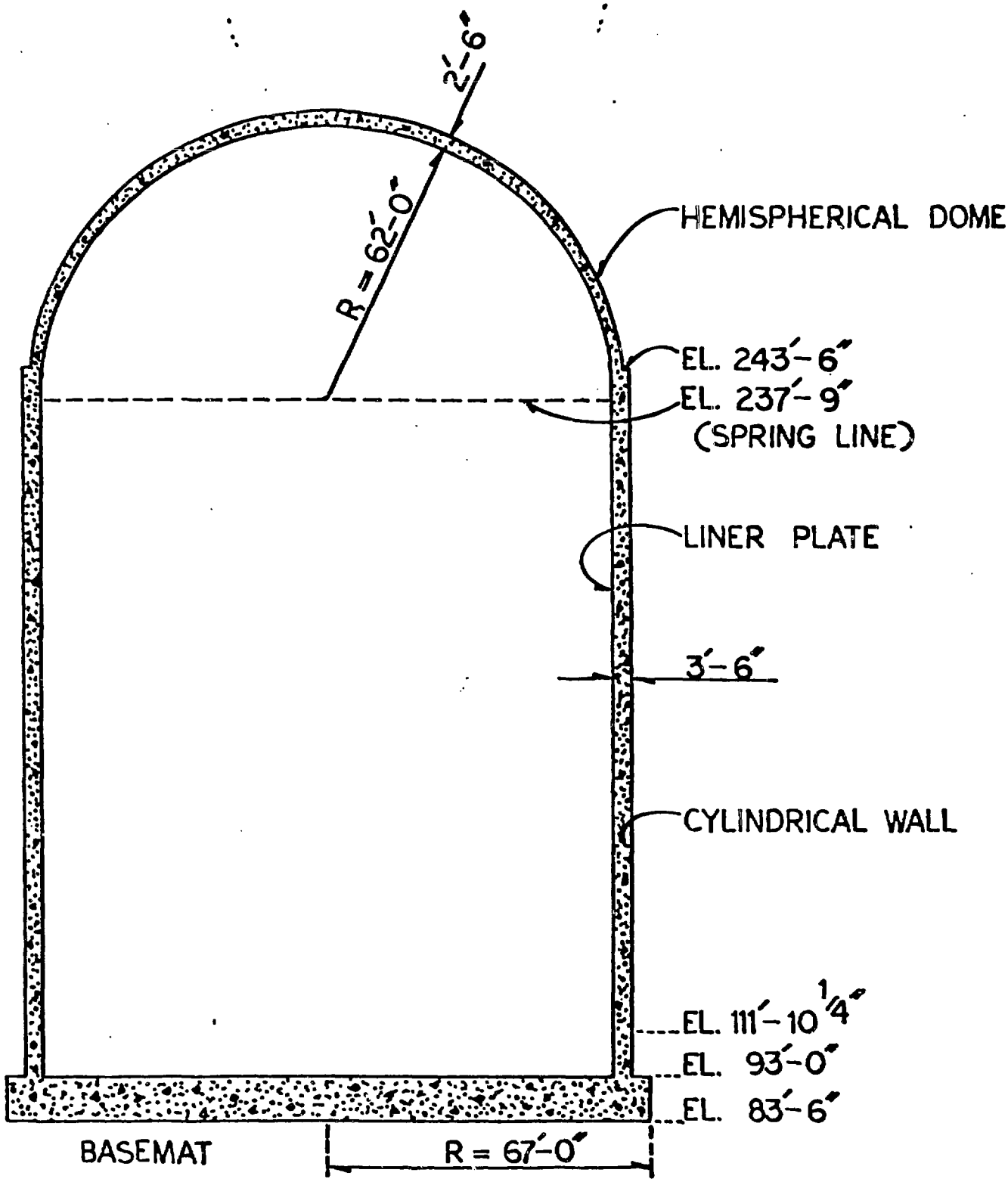

Figure 1. Grand Guld Mark III Containment Building

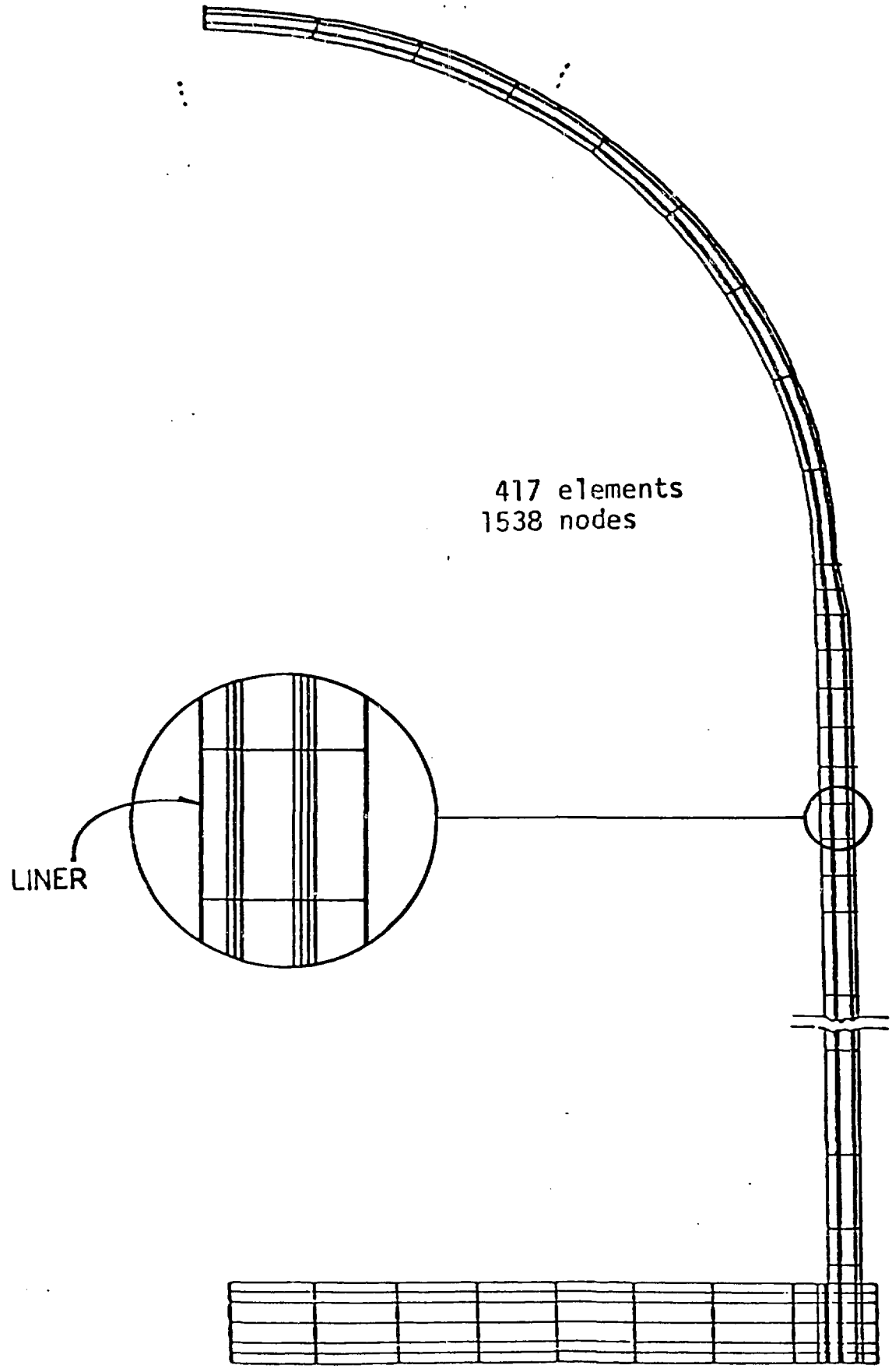

Figure 2. Axisymmetric Finite Element Mesh of the Containment

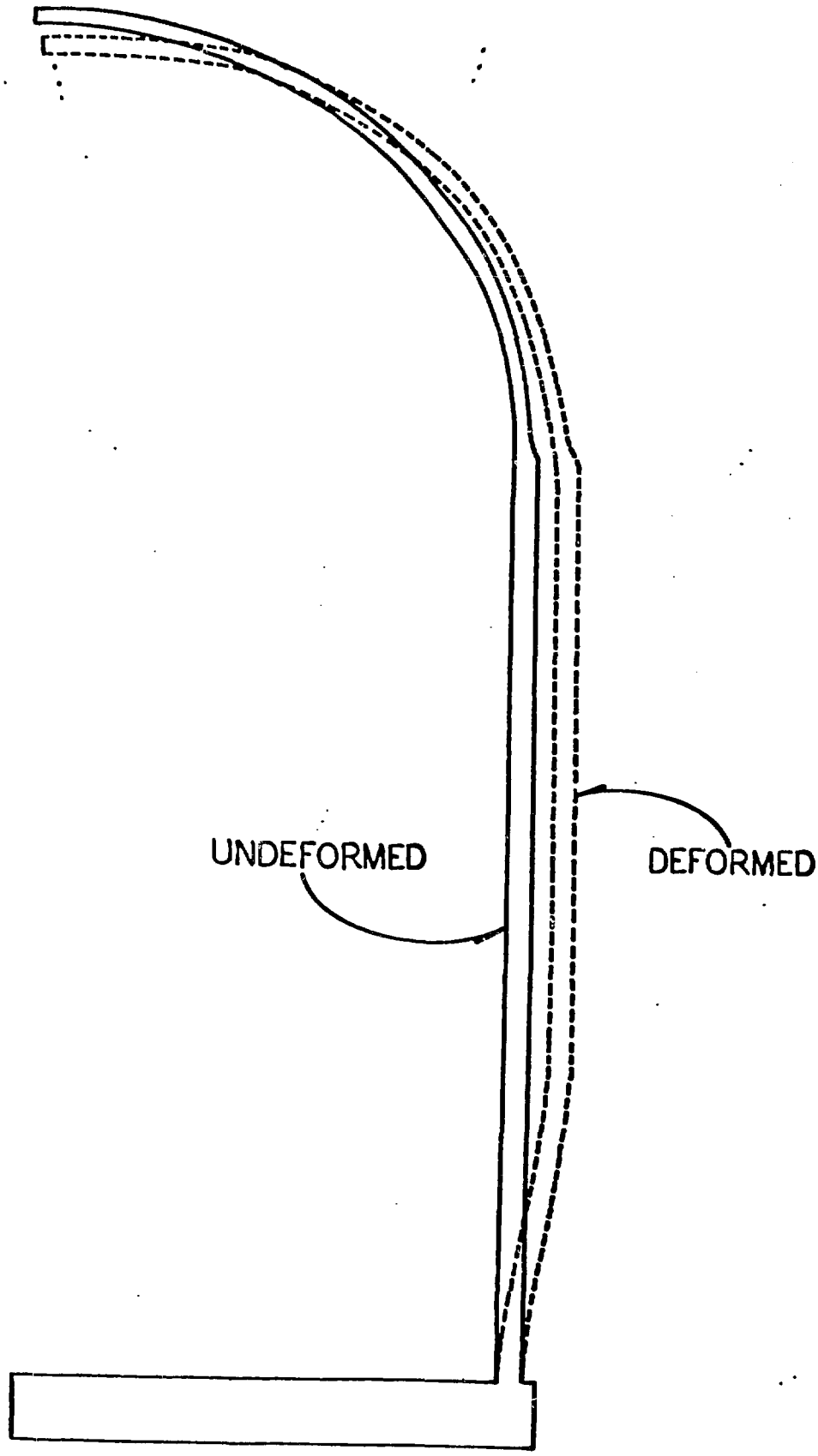

Figure 3. Undeformed and Deformed (at 52 psig) Shapes of the Containment (Displacements Magnified by a Factor of 50)

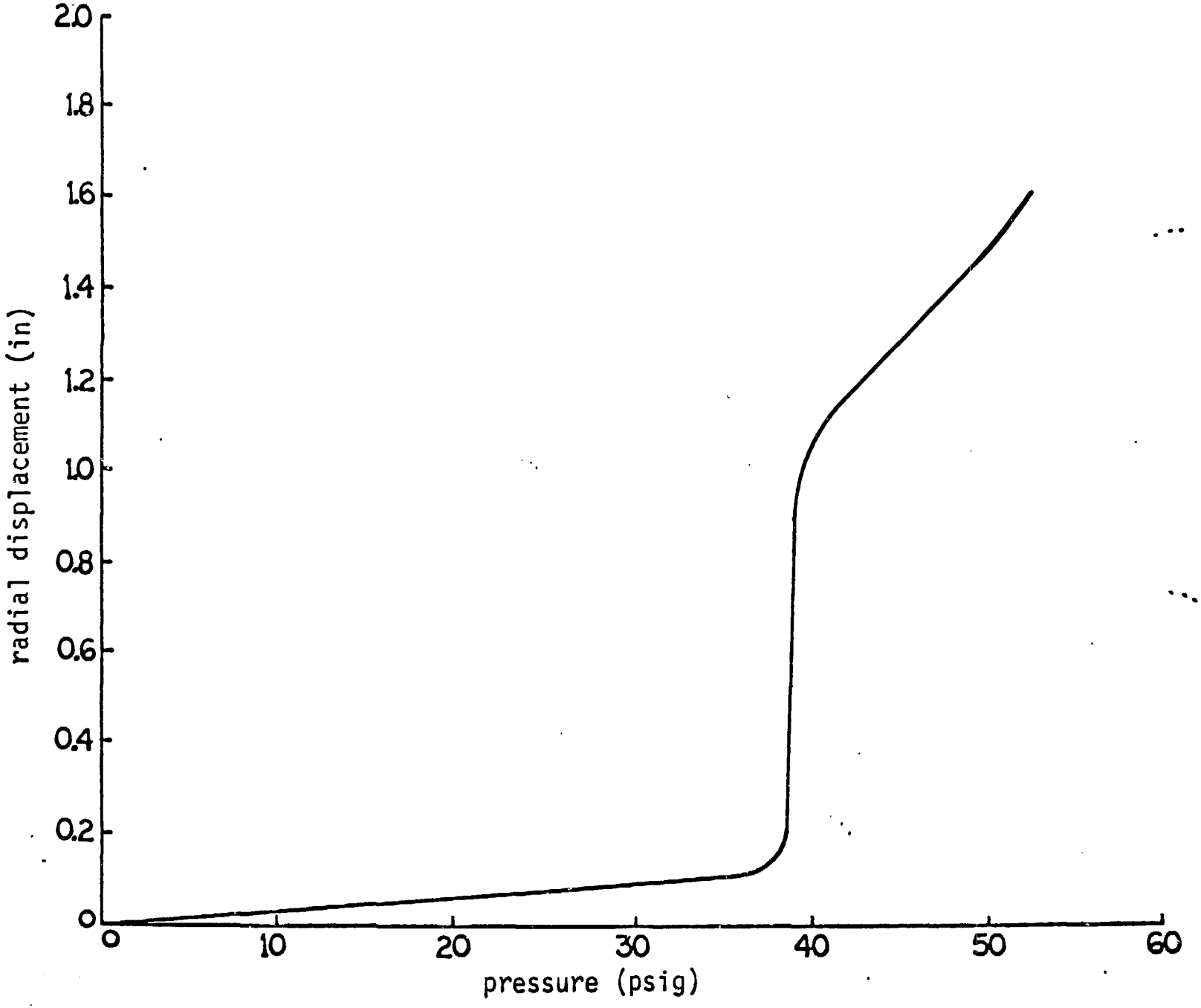

Figure 4. Radial Displacement at Elevation 204' vs. Pressure

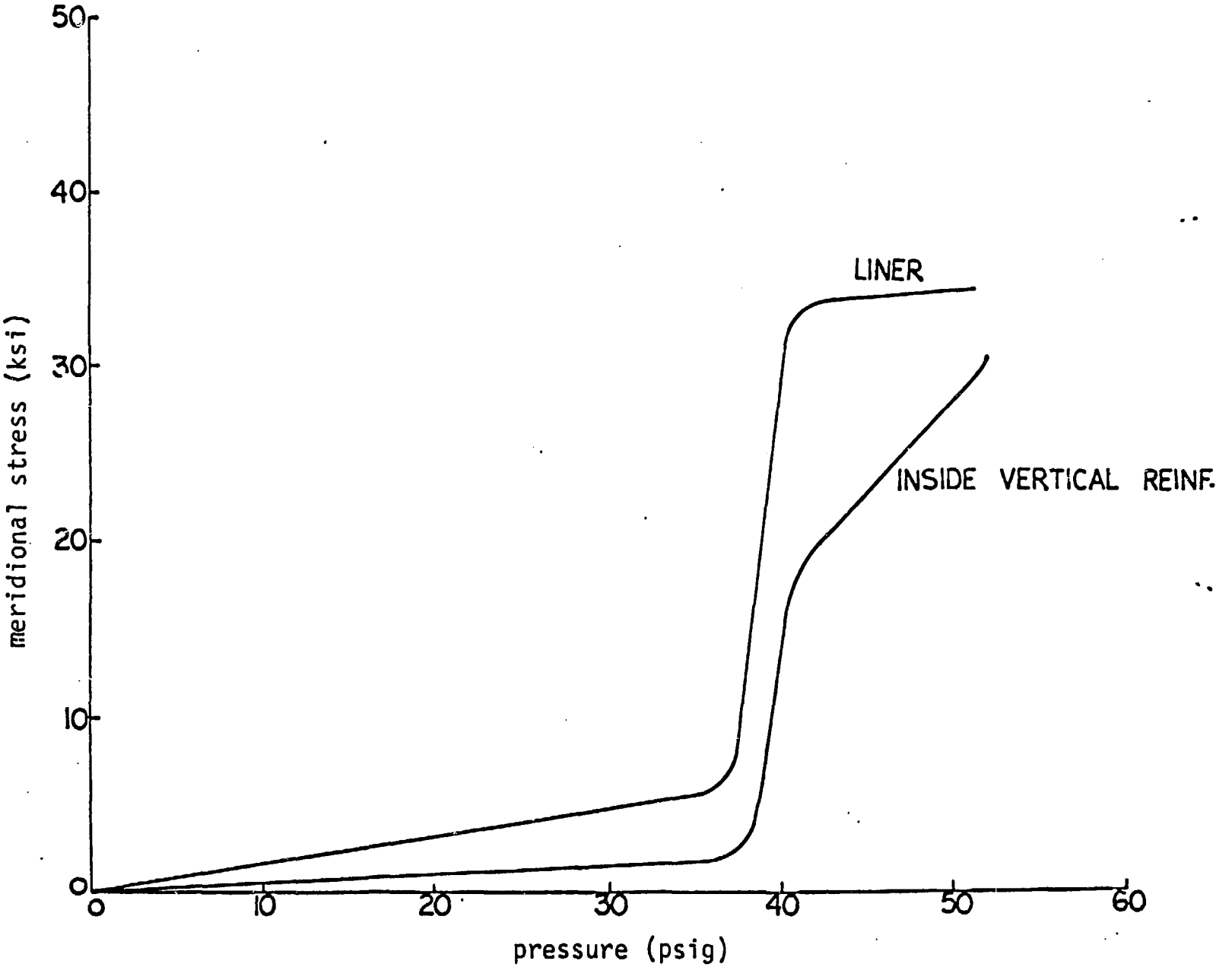

Figure 5. Meridional Stresses at the Mat-cylinder Junction vs. Pressure

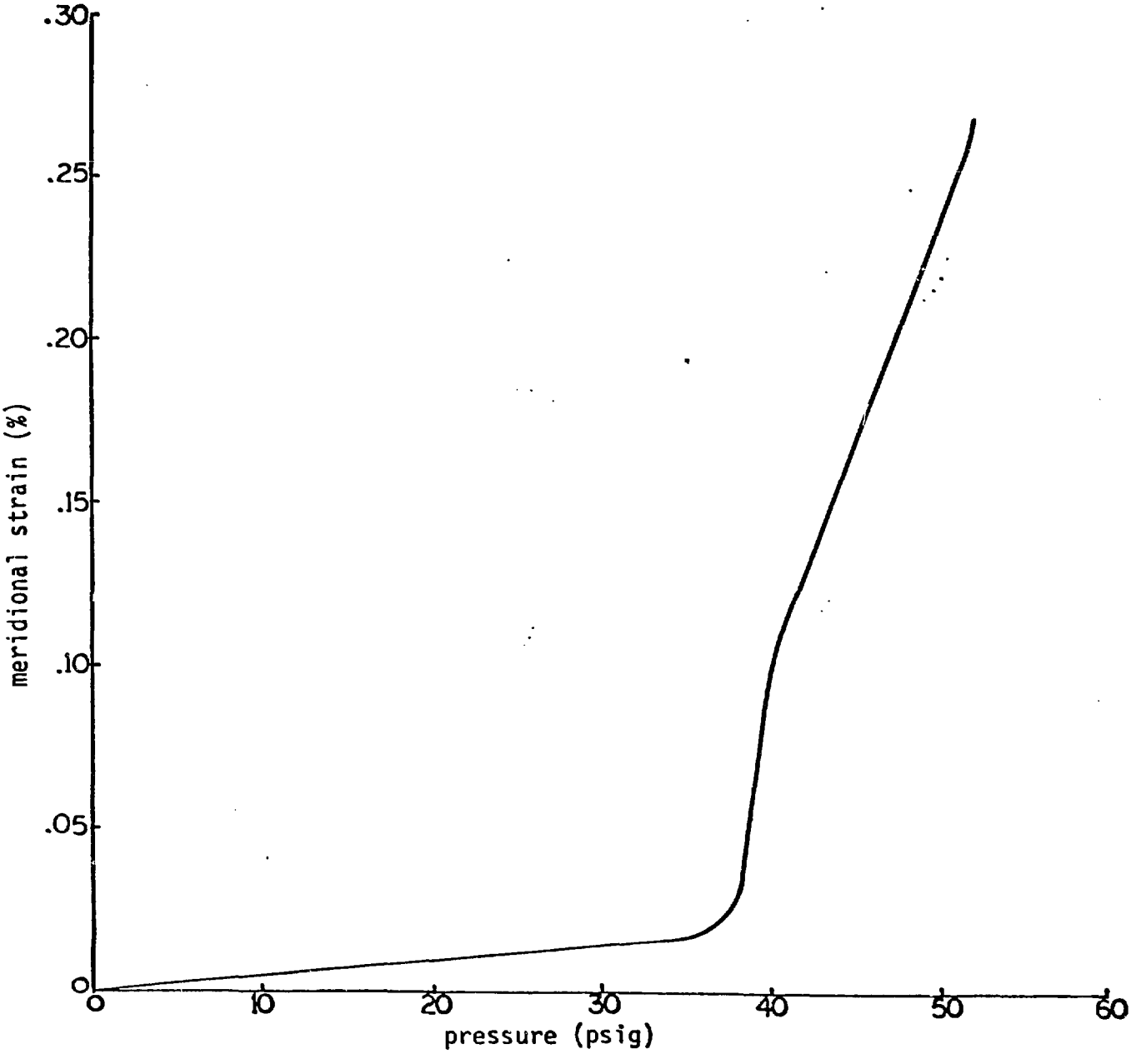

Figure 6. Meridional Strain in the Liner at the Mat-cylinder Junction vs. Pressure

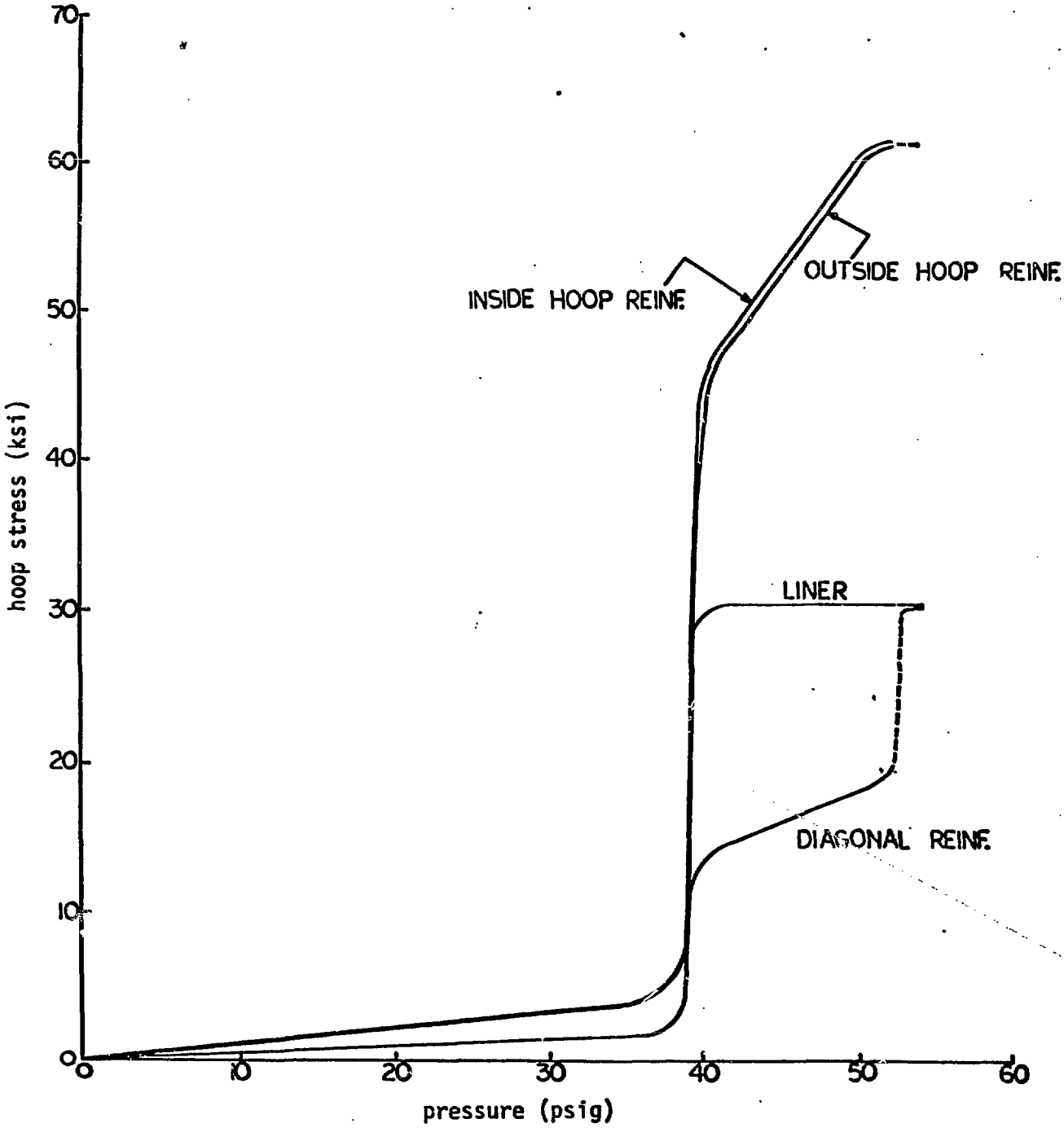

Figure 7. Hoop Stresses at Elevation 207' vs. Pressure

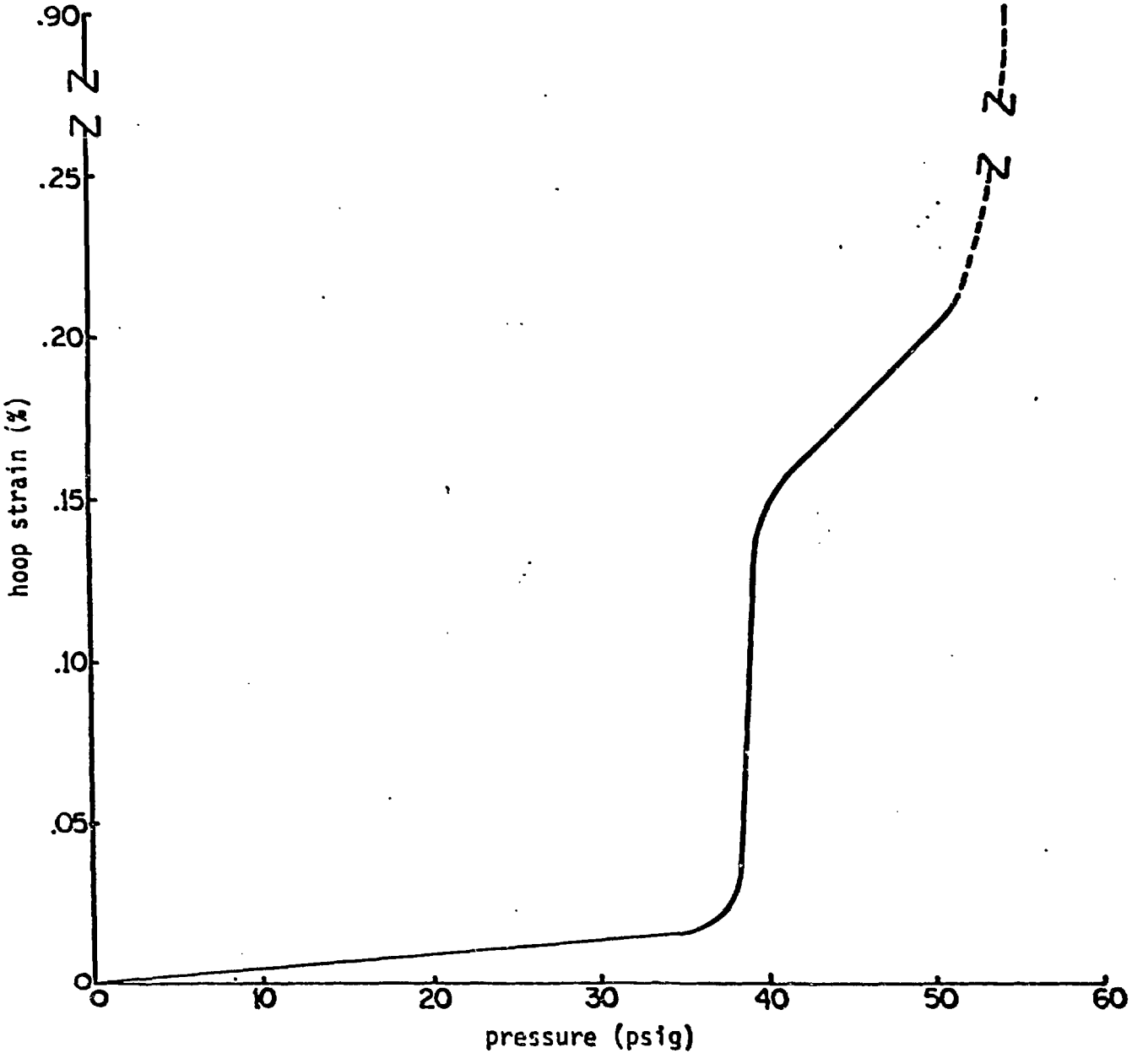

Figure 8. Hoop Strain in the Liner at Elevation 207' vs. Pressure

An analysis of a Mark III reactor-containment vessel subjected to a uniformly increasing internal pressure and gravity loads is carried out in order to ascertain the load-carrying capacity of the structure under hydrogen burn. The analysis is conducted by using a nonlinear finite-element model that includes nonlinearities in the strain-displacement relations as well as in the material constitutive equations. In this analysis, the nonlinear behavior of the liner and reinforcement steels is described by a von Mises elastic-plastic model with isotropic hardening. A recently developed elastic-plastic-fracture model that includes both the cracking and crushing limit states is used for the plain concrete. Consistent smearing and de-smearing procedures are then used to represent the composite material properties of the reinforced concrete by an anisotropic and locally homogeneous continuum.

Results pertaining to the critical regions of the containment where cracking of the concrete, yielding of the reinforcement bars, and substantial straining of the liner take place are discussed in this paper.

1. Introduction

In light water reactors, hydrogen is generated from the primary coolant water during both normal operation and accident conditions. Under normal operation only small amounts of hydrogen are generated and a conventional control system, e.g., the hydrogen recombiner, provides the safe-guard required to control its accumulation. However, during an accident that involves core heat-up, large amounts of hydrogen gas may be produced due to the reaction between water and metals at high temperatures. It is then possible that the hydrogen could escape from the primary vessel and subsequently mix with the oxygen in the containment building to create a mixture which is highly flammable or explosive. The point of concern is: should a LOCA occur and the hydrogen gas ignite, can the concrete containment sustain the extreme pressure and maintain its intended structural integrity? In order to answer this question, structural analysis for predicting the failure of the reinforced concrete containment must be performed for a postulated hydrogen burn.

The nuclear containment vessel is a rather complex, heterogeneous structure composed of an internal steel liner and reinforced concrete walls. The principal function of the steel liner is to provide air-tightness to the containment, whereas the reinforced concrete carries the majority of the structural loads. In the event of a hydrogen burn, the liner may deform excessively and lose its intended function. Also, the concrete may crack which will, in turn, cause plastic yielding of the reinforcements and eventual failure of the structure. This paper describes the results of a nonlinear finite element analysis which was carried out for the Grand Gulf Mark III Reactor Containment Vessel. The purpose of the analysis was to predict the failure pressure capacity of the containment corresponding to maximum allowable strain in the liner and plastic yielding of the reinforcements.

2. Containment Structure

The Grand Gulf Mark III Containment Building (Fig. 1) is a reinforced concrete structure consisting of three basic parts: (1) a base mat, (2) a cylindrical wall, and (3) a hemispherical dome. The base mat, which supports the containment wall and the internal structures, is a flat circular slab with a thickness of 9'-6" and a radius of 67'. The cylindrical wall has an inner radius of 62' and a height of 144'-9" from the top of the mat to the cylinder-dome junction (spring line). The wall thickness is 3'-6" except in some local regions where the thickness is increased to accommodate additional steel reinforcements. The hemispherical dome has the same inner radius (62') as the cylindrical wall but has a reduced wall thickness of 2'-6". The inside surface of the containment is lined with 1/4" thick ductile steel liner plate fabricated from ASTM A-240 Type 304 stainless steel at the bottom 18'-10" of the cylinder, and from ASTM A-285 steel over the remaining height.

The containment is reinforced with ASTM 615 Grade 60 (nominal yield stress 60 ksi) reinforcement bars of varying sizes, e.g., #18, #14, #12, #11 and #10. The primary membrane reinforcement in the cylindrical wall and dome is divided into two groups which are placed near the inside and outside faces of the containment. Each group consists of two layers of bars which provide reinforcements in both the hoop and meridional directions. Another layer of helical (diagonal) bars is placed near the inside face at $+45^{\circ}$ and -45° with the vertical axis to resist the in-plane seismic forces. Further details of the containment reinforcement can be found in references [1] and [2].

3. Material Models

In order to predict the containment failure response, nonlinear material models must be used to describe the stress-strain behavior of the liner and reinforcement steels, the plain concrete and the reinforced concrete. The material models used in the present finite element analysis are briefly discussed in this section.

3.1 Steels

A von Mises plasticity model with an isotropic strain hardening rule was adopted to represent the nonlinear response of liner and reinforcement steels. Since this is a well-known material model [3], only the major equations are briefly outlined.

Under the influence of current stresses σ_i, $i = 1, 2, \ldots 6$, the state of deformation of a steel element is defined by a loading function f_s of the form

$$f_s = \frac{1}{2} S_i^T S_i - \kappa^2 = 0 \tag{1}$$

where S_i and S_i^T denote the stress deviator and its transpose, respectively, and κ represents the radius of the loading surface. For strain-hardening material, κ is a function of plastic work, W^P:

$$\kappa = \kappa (W_p) \tag{2}$$

and

$$W_p = \int \sigma_i \, d\varepsilon_i^P \tag{3}$$

where ε_i^P are the plastic strain components.

The incremental plastic strain components are given by the following flow rule

$$d\varepsilon_i^P = d\lambda \frac{\partial f}{\partial \sigma_i} \tag{4}$$

where $d\lambda$ is a plastic parameter. Following the standard procedure used in plasticity theory, an incremental stress-strain relation in matrix form can be derived from eqs. (2) to (4) as

$$\{d\sigma\} = \left[C_{EP}^1\right] \{d\varepsilon\} \tag{5}$$

where $\left[C_{EP}^1\right]$ is an elastic-plastic matrix of the steel element.

3.2 Plain Concrete

The nonlinear material behavior of plain concrete is characterized by two main features: i) some plastic deformation before crushing under high compressive stresses, and ii) cracking under relatively low tensile stresses. The modeling of these features by an elastic-plastic model combined with a fracture criterion for crushing and cracking is briefly described as follows.

Elastic-plastic Model - An elastic-plastic model originated by Chen and Chen [4] was used in the present analysis since it predicts the nonlinear concrete behavior with sufficient accuracy, and is simple to implement in a finite element program. This model defines two different but similar loading functions to describe the yielding of concrete in different stress regions.

Compression-compression stress state:

$$f_c = \frac{J_2 + (\beta/3) I_1}{1-(\alpha/3) I_1} = \tau^2 \tag{6}$$

Tension-compression or tension-tension stress state:

$$f_c = \frac{J_2 - \frac{1}{6} I_1^2 + (\beta/3) I_1}{1 - (\alpha/3) I_1} = \tau^2 \qquad (7)$$

where α and β are material constants and τ is a strength parameter [4]. J_2 is the second invariant of stress deviator, and I_1 is the first invariant of stress components. With this loading function and the flow rule given by eq. (4), an incremental stress-strain relationship for the concrete can be derived as

$$\{d\sigma\} = \left[C_{EP}^2\right] \{d\varepsilon\} \qquad (8)$$

where $\left[C_{EP}^2\right]$ is an elastic-plastic material matrix for the concrete [4].

Fracture of Concrete - A dual fracture criterion in terms of both stresses and strains is used. The stress-based criterion is obtained simply by assigning $\tau = \tau_u$ in eqs. (6) and (7), where τ_u represents the ultimate strength of concrete under multi-axial stresses. The strain-based criterion is assumed to have the form

$$g(\varepsilon_i) = J_2(\varepsilon) + \frac{A_u}{3} \frac{\varepsilon_u}{f_c'} I_1(\varepsilon) = (\tau_u)^2 \left(\frac{\varepsilon_u}{f_c'}\right)^2 \qquad (9)$$

or

$$\varepsilon_{max} = \varepsilon_t \qquad (10)$$

where $J_2(\varepsilon)$ is the second invariant of strain deviator; I_1, the first invariant of strain components; f_c', uniaxial compressive strength of concrete; A_u, a material constant; ε_u, ultimate compressive strain; ε_t, ultimate tensile strain and ε_{max}, maximum principal strain obtained from the analysis.

3.3 Reinforced Concrete

A computationally efficient approach of modeling the composite nonlinear material behavior of reinforced concrete is to replace this heterogeneous material by an equivalent homogeneous (smeared) material. A smearing procedure is used to derive the constitutive matrix of the homogeneous material in terms of the constitutive matrices of steel and concrete. After the overall deformation of the homogenized material is found, a de-smearing procedure (an inverse process to the smearing procedure) is applied to calculate stresses and strains in both the steel reinforcement and concrete. These stresses and strains are then used to assess the yielding of steel or fracture of concrete. These procedures are described in detail in [5].

The constitutive models and smearing and de-smearing procedures were implemented into a general purpose finite element code NFAP [6], for conducting ultimate strength analysis of concrete containments. Input data for various material parameters used in this code are given in [2].

4. Finite Element Model

The containment geometry is assumed to be axisymmetric in order to develop a finite element model of manageable complexity and size. The effect of containment penetrations, which are small compared to the containment size, is ignored. All steel reinforcements in the containment are also assumed to be axisymmetric. This assumption is justified in view of the smearing and de-smearing procedures used for modeling the reinforced concrete.

The finite element model of the containment is shown in Fig. 2. The containment model consists of 417 eight-noded axisymmetric elements and 1538 nodes. It has seven layers of

elements in the base mat and nine layers in both the cylindrical wall and the hemispherical dome. Different element layers are used to represent the liner plate, the plain concrete, and the reinforced concrete. For example, the nine layers in the containment wall are arranged as: liner plate, plain concrete, hoop-reinforced concrete, vertically reinforced concrete, diagonally reinforced concrete, plain concrete, vertically reinforced concrete, hoop-reinforced concrete and plain concrete. The dome and the foundation mat have similar arrangements of the element layers. The spacings and sizes of the layers are chosen to closely reflect the actual placement of the reinforcements.

5. Analysis Results

The containment was subjected to uniform internal pressure and gravity loads. The internal pressure was increased in various load steps. Initially, step increments of 5 psig were used. These were subsequently reduced to 1 psig at the initiation of concrete cracking, i.e., at about 35 psig. Within the pressure range from 0 to 35 psig, the global stiffness of the finite element model was reformed at the beginning of each load step. Above the pressure level 35 psig, however, the global stiffness was updated not only at the beginning of each load step, but also after each equilibrium iteration within a load step. A total Lagrangian formulation [7] was used in the analysis to include the effect of geometry nonlinearity (large displacements).

5.1 Overall Deformation Pattern

The overall deformation pattern of the containment is shown in Fig. 3 in which both the undeformed and the deformed (at 52 psig) finite element grids are plotted. For clarity, the deformed finite element grid was obtained by multiplying the displacements by a factor of 50. As can be observed from this figure, the bending deformations are comparatively large at the junction of the cylindrical wall and the base mat, and radial displacements are large in the upper half of the cylindrical wall. Negative normal displacements near the crown of the hemispherical dome are caused by the bulging out of the cylindrical wall.

To illustrate the growth of deformation field, the radial displacement at elevation 204' versus pressure is shown in Fig. 4. The radial displacement increases slowly and linearly with the pressure up to 35 psig. Nonlinearity in the displacement pressure curve begins after 35 psig due to the onset of cracking in the concrete. The radial displacement increases very sharply between 38 and 40 psig as large sections of concrete crack in tension and the liner yields. Above 40 psig, additional cracking of the concrete and yielding of the liner tend to level off resulting in a more gradual growth of the displacement.

5.2 Cracking

Cracking in the concrete is governed by the strain criterion for concrete fracture with a maximum allowable tensile strain of 0.015% (see eq. 10). Cracks due to hoop stresses (hoop cracks) begin to appear in several elements of the cylindrical wall at 36 psig. Cracks resulting from the meridional stresses (meridional cracks) are initiated at 37 psig in an element of the base mat just below the inside corner joining the inner cylindrical surface and the top of the base mat. As the pressure increases to 40 psig, the hoop cracks spread rapidly covering almost the entire cylindrical wall, but the meridional cracks are confined to a few elements surrounding the inside corner. The cracked region of the containment expands only slightly between 40 and 47 psig with essentially the same crack patterns. Above 47 psig, however, hoop cracks are initiated in most of the hemispherical dome, and meridional cracks begin to appear in the region above the base of the dome. At 52 psig, the hoop cracks cover

not only most of the cylindrical wall but also the hemispherical dome. The meridional cracks are confined to the hemispherical dome, and to a few elements of the cylindrical wall and the base mat surrounding the inside corner.

5.3 Stresses and Strains at the Mat-Cylinder Junction Region

The mat-cylinder junction is subjected to high meriodional strains and stresses due to the large bending deformations. Figure 5 shows that meridional stresses in both the liner and reinforcement grow linearly at a slow rate until meridional cracks begin to develop at 37 psig. These stresses, however, increase very sharply between 37 and 40 psig as progressive cracking of the concrete releases most of its mericdional stresses. The liner becomes plastic at 40 psig and has an almost flat response above this pressure. After the liner is plastic, additional meridional stresses in tension are carried mainly by the inside vertical reinforcement. At 52 psig, the maximum meridional stress in the vertical reinforcement is 30.5 ksi which is approximately one-half of its nominal yield strength (60 ksi). The variation of liner strain (meridional) with respect to the internal pressure is shown in Fig. 6. The strain is quite small before the concrete cracks, but it increases rapidly with pressure both during and after the cracking. Between 40 and 50 psig, the liner strain increases approximately by 0.013% for each increment of 1 psig. A higher rate of increase at the tail end of the curve is caused by yielding of the hoop reinforcements in the cylindrical wall.

5.4 Stresses and Strains in the Cylindrical Wall Below the Spring Line

Hoop strains and stresses in the containment are highest below the spring line at an elevation of 207'. For a section at this elevation, hoop stress versus internal pressure curves for the liner, inside and outside hoop reinforcements, and diagonal reinforcement are plotted in Fig. 7. As expected, all hoop stresses are low and increase linearly with pressure before the onset of hoop cracks in the concrete. There are, however, large increases in their values between 36 and 40 psig as the stresses from the cracked concrete are transferred to the liner and the reinforcements. At 40 psig hoop stress in the liner reaches 30 ksi, carrying the liner well into plastic zone. Hoop stress in the inside hoop reinforcement attains a slightly higher value than that in the outside hoop reinforcement, especially during the cracking of concrete. These two stresses, however, tend to converge to approximately the same value, 61 ksi, after plasticity develops in both inside and outside hoop reinforcements at 51 and 52 psig, respectively. Hoop stress in the diagonal reinforcement is comparatively lower, but it shows a sharp upturn after 50 psig as the hoop reinforcements begin to yield. At 52 psig, hoop stress in the diagonal reinforcement is 20 ksi. It should be noted that the maximum stress in the diagonal reinforcement is along the reinforcement direction, and is approximately twice the magnitude of hoop stress (e.g., 40 ksi at 52 psig).

The amount of diagonal reinforcement is rather small when compared to the other reinforcements in the containment. Thus, it is apparent that once the liner and hoop reinforcements are fully plastic, the structural stiffness will be reduced by a very significant amount. Indeed, this was the case when the pressure was increased from 51 to 52 psig. The solution convergence after 52 psig would, because of the yielding of the hoop reinforcements, require extremely small load steps. This situation would become even more acute when the diagonal reinforcement is also plastic. Although numerical results above 52 psig were not obtained because of the computational costs, a rough estimate for the yielding of diagonal reinforcement was made based upon the following two assumptions: (1) hoop strain is uniform across the thickness of the wall, and (2) rate of growth internal hoop forces (hoop stress

resultant) with respect to pressure does not change appreciably after 52 psig. With these assumptions, it was determined that yielding would occur between 53 and 53.5 psig as shown by the dotted line in Fig. 7.

Hoop strain versus pressure curve for the liner (at elevation 207') is shown in Fig. 8. The hoop strain jumps from 0.015% to 0.15% as the pressure rises from 36 to 40 psig. Beyond 40 psig the strain grows at a moderately high rate reaching 0.2% at 49.5 psig. Yielding of the hoop reinforcements after 50 psig causes a further increase in the strain growth rate, and the strain reaches 0.215% at 52 psig. Rough estimates were also made for the liner hoop strain for pressure values above 52 psig. Using the two assumptions mentioned above, it can be shown that the hoop strain would increase approximately 0.024% per psig before full yielding of the diagonal reinforcement takes place. However, once the diagonal reinforcement has yielded, the strain would increase at an excessively high rate of roughly 0.65% per psig because of a very low strain hardening of the liner and reinforcement steels. These results are depicted as the dotted portions of the curve in Fig. 8.

6. Summary and Conclusions

In summary, the results of the containment analysis indicate that the cracking of concrete is initiated at 36 psig and that large sections of the concrete will have cracked at 40 psig. Above 40 psig, hoop stresses in the cylinder are resisted mainly by the reinforcements which are still elastic. The inside and outside hoop reinforcements respectively become plastic at 51 and 52 psig. Finally, the diagonal reinforcement also becomes plastic at approximately 53.5 psig. At this juncture in the loading, the liner hoop strain below the spring line will increase at a rate of about 0.65% per psig increment, reaching 0.9% at about 54.5 psig. In view of the large strains which would result in a radial movement of approximately 6.7" at 54.5 psig and an additional movement of 4.8" per psig at higher pressures, the liner integrity above 54.5 psig internal pressure becomes questionable.

References

[1] Structural design drawings, Nos. C-1000 Rev. 2, C-1024 Rev. 8, C-1033 Rev. 13 and C-1036 Rev. 6, Bechtel Power Division, Gaithersburg, MD, (these drawings were provided informally for this study by staff members of the NRC Structural Engineering Branch).

[2] SHARMA, S., REICH, M., CHANG, T. Y., SHTEYNGART, S., "Failure Evaluation of a Reinforced Concrete Mark III Containment Structure Under Uniform Pressure", BNL-NUREG 51543, NUREG/CR-1967 (September, 1982).

[3] ZIENKIEWICZ, O. C., The Finite Element Method, Third Edition, McGraw-Hill, 1977.

[4] CHEN, A. C. T., CHEN, W. F., "Constitutive Relations for Concrete", Journal of the Engineering Mechanics Division, ASCE, No. EM4, Proc. Paper 11529, 101, 465-481 (1975).

[5] CHANG, T. Y., AOKI, H., "A Constitutive Model for Structural Analysis of Fusion Magnets", Nuclear Engineering and Design 58, 237-245 (1980).

[6] CHANG, T. Y., SHARMA, S. K., REICH, M., "A Nonlinear Finite Element Analysis Program-NFAP, Vol. 1 - General Description and Sample Problems", in print.

[7] BATHE, K. J., OZDEMIR, H., WILSON, E. L., "Static and Dynamic Geometric and Material Nonlinear Analysis", UC SESM 74-4 (February, 1974).